



Injectable bone cement with magnesium-containing microspheres enhances osteogenesis via anti-inflammatory immunoregulation

Shenglong Tan^{a,b,c,1}, Yifan Wang^{a,b,c,1}, Yingying Du^{a,b,c,*}, Yin Xiao^{d,e,**}, Shengmin Zhang^{a,b,c,***}

^a Advanced Biomaterials and Tissue Engineering Center, Huazhong University of Science and Technology, Wuhan, 430074, China

^b Department of Biomedical Engineering, Huazhong University of Science and Technology, Wuhan, 430074, China

^c Institute of Regulatory Science for Medical Devices, Huazhong University of Science and Technology, Wuhan, 430074, China

^d Institute of Health and Biomedical Innovation, Queensland University of Technology, Brisbane, 60 Musk Ave, Kelvin Grove, Brisbane, Queensland, 4059, Australia

^e Australia-China Centre for Tissue Engineering and Regenerative Medicine, Queensland University of Technology, 60 Musk Ave, Kelvin Grove, Brisbane, Queensland, 4059, Australia

ARTICLE INFO

Keywords:

Injectable bone cement microsphere
Mg
Immunomodulation
Anti-inflammation
Osteogenesis

ABSTRACT

Injectable bone cement is especially useful in minimally invasive surgeries to repair small and irregular bone defects. Amongst different kinds of injectable bone cements, bioactive calcium phosphate bone cement (CPC) has been widely studied due to its biological activity. However, its dense structure and poor biodegradability prevent the ingrowth of living tissue, which leads to undesirable bone regeneration and clinical translation. To address this issue, we prepared bone cement based on Magnesium-containing microspheres (MMSs) that can not only be cured into a 3D porous scaffold but also have controllable biodegradability that continuously provides space for desired tissue ingrowth. Interestingly, magnesium ions released from MMSs cement (MMSC) trigger positive immunomodulation via upregulation of the anti-inflammatory genes IL-10 and M2 macrophage polarization with increased expression of CD206, which is beneficial to osteogenesis. Moreover, the physicochemical properties of MMSC, including heat release, rheology and setting time, can be tuned to meet the requirements of injectable bone cement for clinical application. Using a rat model, we have demonstrated that MMSC promoted osteogenesis via mediation of tissue ingrowth and anti-inflammatory immunomodulation. The study provides a paradigm for the design and preparation of injectable bone cements with 3D porous structures, biodegradability and anti-inflammatory immunoregulation to efficiently promote osteogenesis.

1. Introduction

Among the numerous bone implant materials, injectable bone cement has been the most widely used for filling and repairing orthopaedic traumas, especially those with irregular shapes, in minimally invasive surgery [1] due to its excellent mouldability. However, the most commonly used injectable bone cement in the clinic, whether primitive bioinert polymethylmethacrylate (PMMA) cement [2] or current bioactive calcium phosphate cement (CPC) [3,4], has difficulties

in forming an interconnected porous structure in situ. As is known that the porous structure can reserve space for cell attachment, ingrowth, and subsequent osteogenic differentiation and vascular remodelling [5]. Without porous structure, cell ingrowth, blood vessel invasion, and new bone formation will be purely dependent on only the degradation of bone cement itself. However, currently commercialized CPC has a very low and uncontrollable biodegradability [6], which makes CPC an impregnable block mass. Regardless of the biocompatibility and osteoconductivity, current CPC usually results in a long-term foreign body

Peer review under responsibility of KeAi Communications Co., Ltd.

* Corresponding author. Advanced Biomaterials and Tissue Engineering Center, Huazhong University of Science and Technology, Wuhan, 430074, China

** Corresponding author. Institute of Health and Biomedical Innovation, Queensland University of Technology, Brisbane, 60 Musk Ave, Kelvin Grove, Brisbane, Queensland, 4059, Australia

*** Corresponding author. Advanced Biomaterials and Tissue Engineering Center, Huazhong University of Science and Technology, Wuhan, 430074, China

E-mail addresses: yingyingdu@hust.edu.cn (Y. Du), yin.xiao@qut.edu.au (Y. Xiao), smzhang@hust.edu.cn (S. Zhang).

¹ These authors contributed equally to this work.

<https://doi.org/10.1016/j.bioactmat.2021.03.006>

Received 6 January 2021; Received in revised form 23 February 2021; Accepted 2 March 2021

2452-199X/© 2021 The Authors. Publishing services by Elsevier B.V. on behalf of KeAi Communications Co. Ltd. This is an open access article under the CC

BY-NC-ND license (<http://creativecommons.org/licenses/by-nc-nd/4.0/>).

reaction and wrapped in new bone tissue. To address these issues, strategies have been implemented to mix CPC with magnesium phosphate cement (MPC).

MPC is known for its ability to set quickly, its high strength and rapid biodegradation [7]. More importantly, as an essential element of human body, magnesium (Mg) participates in many important physiological processes, including the maintenance of hormone levels [8], immune responses [9,10] and promotion of bone formation [11]. Macrophages play an important role in the immune response induced by xenogenous implants [12]. Generally, macrophages can be activated to a pro-inflammatory (M1) phenotype, releasing cytokines and chemokines, or a regulatory constructive (M2) phenotype, which has been found to be associated with immunoregulation and the transition of pro-inflammatory status to tissue reconstruction [13]. Modulating macrophage polarization towards a balanced M1/M2 or predominantly M2 phenotype following implantation can improve the implantation outcomes. Previous studies have reported that Mg-containing bone implants, such as β -TCP-coated Mg metal [14] and MgSiO_3 -coated hydroxyapatite [15], were able to induce M2 polarization of macrophages and subsequent osteogenesis. These findings not only shed light on the importance of Mg in implant-bone interactions but also led to the hypothesis that Mg-containing cements may also result in an M2 phenotype macrophage-dominated immune response with enhanced bone regeneration. Thus, the addition of MPC to CPC is expected to introduce not only a short setting time and applicable biodegradability [16] but also better bioactivity due to the immune regulation of Mg.

However, given that the starting materials of CPC and MPC are powder, the composite bone cement formed after setting cannot form a connected porous structure in the subsequent degradation process. Thus, to obtain porous scaffolds, an additional pore forming process must be introduced, such as the NaCl particle leaching procedure [18]. Although these methods were partially effective, they could not change the fact that the cured cement is still a block mass. Moreover, considering the practical application, it is necessary to develop an injectable bone cement that can form a porous structure in situ. To the best of our knowledge, to date, no Mg-containing injectable bone cement can be cured in situ into a highly biodegradable porous structure.

Over the past few years, 3D printing and other additive manufacturing technologies have shown unique advantages for tissue engineering. In our previous study, PCL and calcium phosphate complex microspheres can be moulded into porous scaffolds with arbitrary

shapes by melting and fusing the contact interface between each adjacent microsphere by selective laser sintering [17]. Inspired by this, we propose that shaping the precursors of Mg-containing injectable bone cement to form microsphere might be an ingenious way to create an injectable porous scaffold. The microspherical morphology can endow Mg-containing injectable bone cement with good rheological properties, thereby improving the injectability. The curing reaction can be restrained to the contact interface of the microsphere, thus slowing the reaction rate and reducing the exotherm. The gaps between microspheres can form connected pores, leaving space for cell migration and tissue infiltration. More importantly, through biodegradation and release of magnesium ions, it can provide space for more tissue ingrowth and exerts immunomodulation for M2 phenotype polarization of macrophages, thereby triggering angiogenesis and new bone formation (Fig. 1).

Herein, an injectable bone cement was developed based on Mg-containing microspheres (MMSs) in this study. The major component of MMSs was MgO, which was the same as MPC, substantially guaranteeing a rapid curing of MMSs bone cement (MMSC). The minor components were MgSiO_4 and $\text{Ca}_7\text{Mg}_2\text{P}_6\text{O}_{24}$. MgSiO_4 could maintain the morphological structure after curing in situ [21,22], whereas the $\text{Ca}_7\text{Mg}_2\text{P}_6\text{O}_{24}$ could reduce the exotherm during the curing process of MMSC. The physicochemical characteristics, including injectability, exothermic properties, ion release and biodegradability of MMSC, were thoroughly studied and compared to those of the CPC and MPC. We also investigated the immunomodulation of Mg^{2+} released from MMSC through inflammatory gene expression and macrophage polarization. The subsequent osteogenesis was studied using a coculture system containing RAW264.7 cells and rat bone marrow mesenchymal stem cells (rbMSCs) under the simulation of MMSC extract. By subcutaneous implantation in rats, the capability of inducing tissue ingrowth, osteoimmunomodulation, and osteogenesis by MMSC was validated *in vivo*.

2. Materials and methods

2.1. Materials

CPC was purchased from Shanghai Rebong Biomaterials Co., Ltd. (China). Magnesium carbonate basic (MgCB) was purchased from Shandong Xiya Chemical Industry Co., Ltd. (China). Recombinant

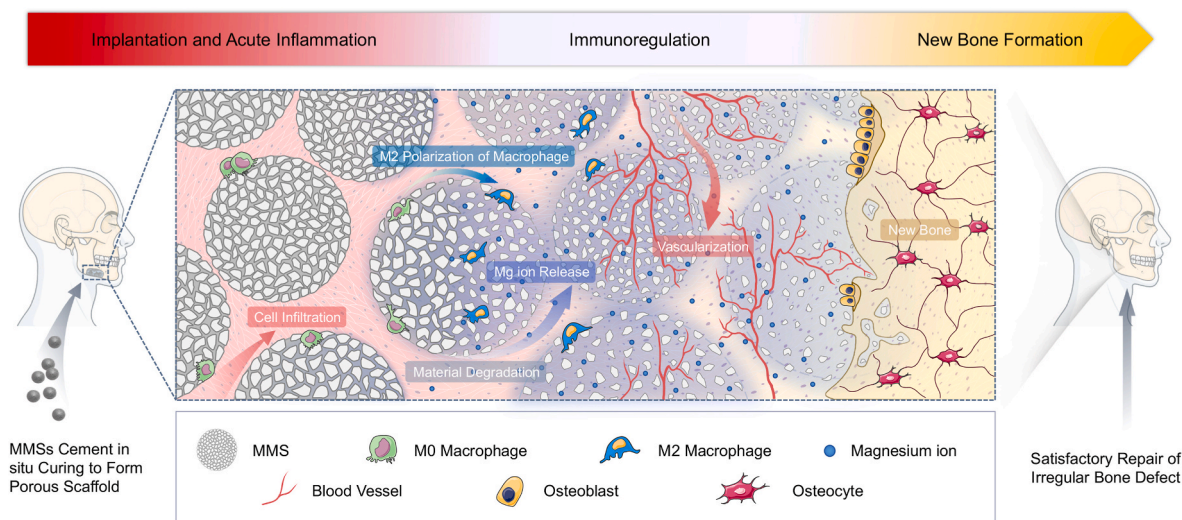


Fig. 1. Schematic illustration for the principles of bone defects filling and repair by MMSC. The MMSs are not only of the desired physicochemical properties to meet the requirement of injectable bone cement for clinical application, but also can be cured into a 3D interconnected porous scaffold conducive to cells and tissue ingrowth in situ. Moreover, the controllable biodegradation of MMSC continuously provides increasing space while the release of magnesium ions induces a tissue repair favourable immunoregulation via the M2 phenotype polarization of macrophages for the consecutive vascularization and new bone formation.

human bone morphogenetic protein 2 (rhBMP 2) was purchased from Beijing Wishbiotechnology Co., Ltd., China. Calcium nitrate, diammonium hydrogen phosphate, dimethyl silicone fluid and tetramethyl silane were all purchased from Sinopharm Chemical Co., Ltd. All reagents and solvents were of analytical grade and were used as received.

2.2. Preparation and characterization

2.2.1. Preparation and characterization of MMSs

MMSs were prepared through a modified liquid drop condensation method. Briefly, amorphous tricalcium phosphate containing silicon dioxide (ACP-Si) was fabricated as described in the literature [16] with a Si content of 3.08 ± 0.2 wt%, and the addition of Si stabilized the microsphere from collapsing [18,19]. Silicones were added into a beaker equipped with a mechanical stirrer and precooled in an ice bath. A slurry of 0.225 g magnesium carbonate basic (MgCB), 0.075 g ACP-Si, 636.7 μ L deionized water and 339 μ L 15 wt% gelatine solution was well mixed at 70 °C and then dropped into silicone with a mechanical stirring speed of 285 rpm. After 40 s, the mechanical stirring was stopped, and the microspheres were collected and crosslinked using a 2.5% v/v glutaraldehyde solution. Then, these crosslinked microspheres were dried at 60 °C to obtain the MMSs precursors. Finally, MMSs were obtained by sintering the MMSs precursors at 1200 °C for 2 h.

The surface morphology and elemental distribution of MMSs were observed by scanning electron microscopy (SEM, FEI, Holland). In detail, MMSs were distributed on carbon conductive adhesive and sputter-coated with a layer of gold for further observation. The pore size distributions and specific surface area of MMSs were characterized by specific surface area and pore size distribution analysis (BET, V-Sorb 2800 TP, Gold APP, Ltd., China). Before the test, 2g of MMSs were dried at 100 °C for 12h. The phase composition of MMSs was analysed by powder X-ray diffraction (XRD, PANalytical, Holland) with Cu K α radiation. For XRD test, MMSs were mashed into powder using a mortar.

2.2.2. Preparation of cement pastes and their setting scaffolds

The ready-to-use MMSC, MPC and CPC pastes were prepared by mixing the MMSs, MgO and CPC powder with the setting solution at liquid-to-solid ratios (L/S) of 1.73, 2.5 and 0.4 mL/g, respectively. The setting solution used in the MMSC and MPC pastes was saturated ammonium dihydrogen phosphate (NH₄H₂PO₄) solution. A mixing time of 2 min was chosen following the operation time for clinical application [18]. Subsequently, all the cement pastes were injected into square (4.5 \times 4.5 \times 1 mm), round (\varnothing 5 \times 1 mm) or equilateral triangle (side length: 3.5 mm; thickness: 1 mm) moulds and cured at 37 °C to form cement scaffolds.

2.3. Physicochemical characterization

2.3.1. The temperature evolution

Cement pastes containing 0.1 g of MMSs, MgO or CPC powder were used for this test. After mixing the powder with the setting solution, the temperature evolution during the setting reaction was detected by introducing a type K thermocouple (RS 1313 thermometer) into the cement pastes. Once the solid and liquid were mixed, the time was counted, and the temperature was recorded per minute until room temperature was reached.

2.3.2. Rheological property

For each test, cement pastes containing 2 g of CPC powder or MMSs were prepared by mixing the solid and setting solution for 1 min. The rheological tests were conducted using an ARES-G2 rheometer (TA, Inc.) with cone and plate measuring geometries with diameters of 25 mm and cone angles of 0.1 rad. The test time was set to 30 min, and the shear rate was set to range from 100 s⁻¹ to 10 s⁻¹. The rheological property of MPC was unable to be detected since it had cured before the test due to its fast setting rate.

2.3.3. Determination of the setting time

MMSC, MPC and CPC pastes were placed in a stainless-steel mould (\varnothing 6 \times 12 mm). The samples were tested at various intervals using a Vicat apparatus, which consists of a frame bearing a movable rod weighing 300 g, with a 1 mm stainless-steel needle at the end. According to ASTM Test Method C 187–98 [19], the setting time was determined to be the time taken before the needle was unable to penetrate more than 1 mm into the sample. Each experiment was performed in triplicate, and the average value was calculated.

2.3.4. Ion release and degradation in cell culture medium

Three groups of cements, CPC, MPC and MMSC, were cured in cylindrical mould (\varnothing 5 mm) for 3 days at 37 °C. Then, four samples with an average weight of 0.0758 g per group were immersed in 3 mL DMEM (Low Glucose, Hyclon) at 37 °C. After 12 h, 24 h, 3 days, 7 days, 14 days and 21 days, the solution was collected and refreshed by the addition of 3 mL DMEM. Then, the concentrations of Ca²⁺ and Mg²⁺ in different time intervals were analysed by using inductively coupled plasma-atomic emission spectrometry (ICP-AES, PerkinElmer Optima 2000). The accumulated concentration of calcium and magnesium ions were calculated by subtracting the concentration of calcium and magnesium ions contained in DMEM (Ca²⁺: 72 μ g/mL, Mg²⁺: 19.5 μ g/mL).

Cements were collected at different time intervals and then dried to calculate the weight loss. The weight loss of cements was calculated using the following formula:

$$\text{Weight loss (\%)} = (W_0 - W_t) \times 100/W_0$$

W₀ is the dry weight before degradation and W_t is the dry weight at time t.

2.3.5. Surface morphology and phase transition in vitro and in vivo

MMSC, MPC and CPC scaffolds (0.01 g) were fabricated in a cylindrical mould (\varnothing 5 \times 1 mm) as described in section 2.2.2. After being allowed to set for 3 days, cement scaffolds were soaked in 2 mL DMEM. The DMEM was replaced every two days. Then, the cement scaffolds were collected at 5 and 28 days, followed by washing with deionized water. For the *in vivo* process, the same cement scaffolds were implanted subcutaneously into rats. Then, the implanted cements were collected after 3, 7 and 14 days and fixed using formaldehyde. All collected samples were air dried, and the surface morphology and phase composites were analysed using SEM and XRD.

2.4. In vitro studies

2.4.1. Preparation of cement extracts

MMSC, MPC and CPC pastes were first cured for 3 days and then dried, ground and sieved through a 300-mesh sift. Subsequently, 1 g of cement powder was added to 5 mL DMEM at 37 °C for 24 h. After centrifugation at 5000 rpm for 10 min, the supernatants were collected and filtered through 0.22 μ m filter to obtain cement extracts at a concentration of 200 mg/mL. Then, conditioned media were obtained by diluting with complete medium (DMEM with 10% FBS and 1% penicillin-streptomycin).

2.4.2. RAW264.7 cell proliferation and cytotoxicity

RAW264.7 cells were seeded in 96-well plates at a density of 3×10^4 cells/cm². After 12 h of incubation, the complete medium was replaced with conditioned media. Then, the conditioned media were removed after 1 and 3 days, followed by washing twice with PBS. Subsequently, the cell proliferation rate was evaluated using CCK-8 assay kits (US Everbright, Inc.). Three parallel samples were used in each experimental group, and the optical density (OD) values were recorded by a microplate photometer (EON; Bio-Tek, Winooski, VT, USA) at a wavelength of 450 nm.

Live/dead staining was further conducted to evaluate the

cytotoxicity of conditioned medium. RAW264.7 cells were seeded and incubated as described above. Then, the complete medium was replaced with conditioned medium at a concentration of 3.125 mg/mL. After 2 days of incubation, the cells were stained with a Live/Dead Double Staining Kit (US Everbright, Inc.) following the product instructions. Three parallel samples were used for each experimental group, and three fields of observation from each well were randomly imaged using a fluorescence microscope (Nikon, 80i, Japan). Then, the relative staining areas of dead cells were calculated using ImageJ.

2.4.3. Cytotoxic effects of conditioned medium on rbMSCs

RbMSCs were seeded in 96-well plates at a density of 3×10^5 cells/cm². After 12 h of incubation, the complete medium was replaced with conditioned medium at a concentration of 3.125 mg/mL. Then, after 1 and 3 days, the cytotoxicity was evaluated using CCK-8 assay kits as described in section 2.4.2.

2.4.4. The expression of inflammatory genes by an RT-qPCR assay

RAW cells were seeded in 6-well plates at a density of 5×10^4 cells/cm². Three parallel samples were used for each experimental group. After incubation for 1 day, the complete medium was replaced with conditioned medium. Then, after 2 days, the cells were collected for RT-qPCR to test the expression of the IL6, IL10, CCR7, and CD206 genes. The 2^{-ΔΔCt} method was applied to compare the mRNA expression levels. The primer pairs used in the qRT-PCR were showed in Table S1.

2.4.5. Transwell Co-culture

In the Transwell-24 culture plate (NEST Biotechnology Co. LTD., China), RAW264.7 cells were seeded in the upper chamber with a 0.4 μm polyethylene terephthalate (PET) membrane at 3×10^4 cells/cm², and rbMSCs were seeded in the bottom chamber at 1×10^5 cells/cm². Cells were cultured using complete medium as described in section 2.4.1.

2.4.6. Detection of inflammatory factor proteins

RAW264.7 cells were seeded in the upper chamber of Transwell-24 culture plate with the density of 3×10^4 cells/cm² in conditional medium. Meanwhile, rbMSCs were seeded in 24-well plates with the density of 1×10^5 cells/cm² in complete medium. After incubation for 1 day, the complete medium in 24-well plates was removed and the upper chamber of Transwell-24 culture plate with RAW264.7 cells was transferred to the 24-well plates. Subsequently, coculturing system was established by adding conditioned medium. Then, the conditioned medium was collected after coculturing for 3 days. The concentrations of IL-6 and IL-10 in conditional medium were detected by IL-6 and IL-10 ELISA kits (both purchased from Bio-Swamp, China).

2.4.7. Detection of osteogenic differentiation genes

The expression of osteogenic differentiation genes was determined by an RT-qPCR assay. Similar to the method mentioned in section 2.4.5, RAW264.7 cells and rbMSCs were seeded in Transwell-24 culture plates. After incubation for 1 day, the complete medium was replaced with conditioned medium. Then, after coculturing for 7 days, rbMSCs were collected for the measurement of the gene expression levels of RUNX2 and COL1 by an RT-qPCR assay as described in section 2.4.4. The primer pairs used in the qRT-PCR were showed in Table S1.

2.5. In vivo studies

2.5.1. The fabrication of the implanting cement scaffold

Cement scaffolds were fabricated on cylindrical moulds with diameters of 5 mm and heights of 1 mm. 0.01 g MMSs, MgO and CPC powder were used to prepare the MMSC, MPC and CPC scaffolds according to the method in section 2.2.2. All cement samples were sterilized by autoclaving at 120 °C for 20 min. RhBMP 2-loaded cement scaffolds were obtained by soaking each cement scaffold in 500 μL rhBMP 2 solution at 1 μg/mL.

2.5.2. Surgical procedures

Twenty-four female Sprague-Dawley (SD) rats were employed in this research. The average weight of each rat was approximately 250 g. All animal procedures were approved by the Institutional Animal Care and Use Committee at Huazhong University of Science and Technology. Animals were divided into two groups: half of the rats were implanted with cement scaffolds without rhBMP-2 for short-term immune response, and the other half were implanted with cement scaffolds containing rhBMP-2 for ectopic osteogenesis. Dorsal regions of each rat were shaved and disinfected, and the skin was incised under conditions of general anaesthesia (using 4% chloral hydrate). Then, the implants were inserted, and the surgical cut was closed by suturing.

2.5.3. Histological analysis

Animals were sacrificed with an intraperitoneal injection of excessive amounts of chloral hydrate. Then, the implants with a small amount of surrounding tissue were collected. After fixing in 4% formaldehyde, implants were embedded in PMMA after gradient ethanol dehydration or paraffin embedding after the decalcification process in EDTA solution. Nondecalcified and decalcified sections were cut from the middle of the explants and stained via Masson's trichrome, HE and immunohistochemical staining. Histological observation was performed with a super deep scene 3D microscope (DSX 510, Olympus, USA) and light microscopy.

2.6. Statistical analysis

All data were expressed as the mean ± standard deviation (SD) and analysed using one-way ANOVA analysis, and a p value < 0.05 was considered statistically significant.

3. Results and discussion

3.1. Curing of MMSC generated a 3D porous scaffold

A modified droplet freezing method [20] with gelatine as an original template was employed to fabricate MMSs (Fig. 2a). Before sintering, the MMSs precursor had a spherical morphology with diameters ranging from 700–900 μm (Fig. S1). After sintering, MMSs still had a spherical morphology but with diameters ranging from 300–500 μm (Fig. 2b). TG results suggested that the inorganic component content of the MMSs precursor was approximately 80 wt%, while the gelatine content was only approximately 20 wt% (Fig. S2). Such a high inorganic content might help to maintain the spherical morphology during sintering. We found pores both on the surface and in the interior of the MMSs (Fig. 2b), which could be attributed to the loss of the organic phase during the sintering process. BET characterization demonstrated that the pore diameter mainly ranged from 2–60 nm (Fig. 2c). These nanopores greatly increased the specific surface area of MMSs to 95.86 m²/g (Fig. S3), which could be used to facilitate the loading and release of growth factors and other drug molecules to promote bone repair. EDS-element mapping indicated that the MMSs were a composite of calcium, phosphate, magnesium, silicon and oxygen (Fig. 2d). Phase composition analysis by XRD further demonstrated that the primary phase of the MMSs was MgO (Fig. 2e), which was formed by thermal decomposition of MgCB in the MMSs precursor during the sintering process (Fig. S4). We also found the secondary phases of Ca₇Mg₂P₆O₂₄ and MgSiO₄ (Fig. 2e), which was generated by reacting MgO with silicon containing ACP. The inclusion of the secondary phases may partially play a role as a retardant, slowing down the reaction rate of MgO to control the exotherm during the curing process.

After setting for 12 h, the MMSs could be easily moulded into scaffolds with different shapes (Fig. 3a). More importantly, SEM observation demonstrated many interconnected micropores within the scaffold due to the fusion of the contact interface between adjacent microspheres. The XRD pattern showed a new primary phase of NH₄MgPO₄·6H₂O,

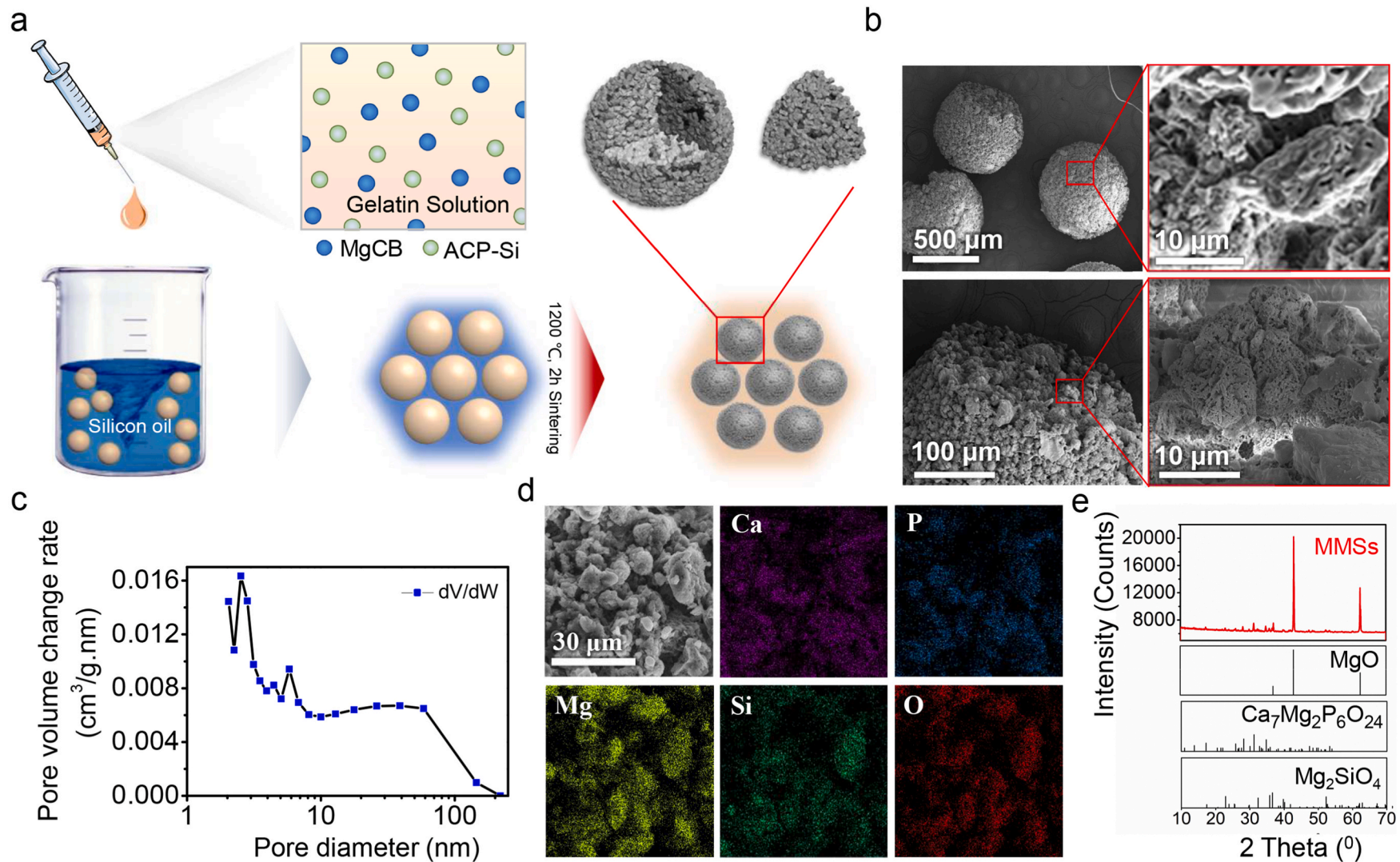


Fig. 2. Preparation and characterization of MMSs. (a) Schematic diagram of the MMSs fabrication process. (b) SEM showed that micropores distributed on the surface and in the interior of the MMSs. (c) BET results indicated that the pore diameters of MMSs mainly ranged from 2–60 nm. (d) The elemental mapping results displayed two distribution areas: Ca–P and Mg–Si–O. (e) XRD patterns showed that the main phase of MMSs was MgO, and the secondary phases were $\text{Ca}_7\text{Mg}_2\text{P}_6\text{O}_{24}$ and Mg_2SiO_4 compared with JCPDS#45–0946, JCPDS#20–0348, and JCPDS#34–0189, which corresponded to MgO, $\text{Ca}_7\text{Mg}_2\text{P}_6\text{O}_{24}$, and Mg_2SiO_4 , respectively.

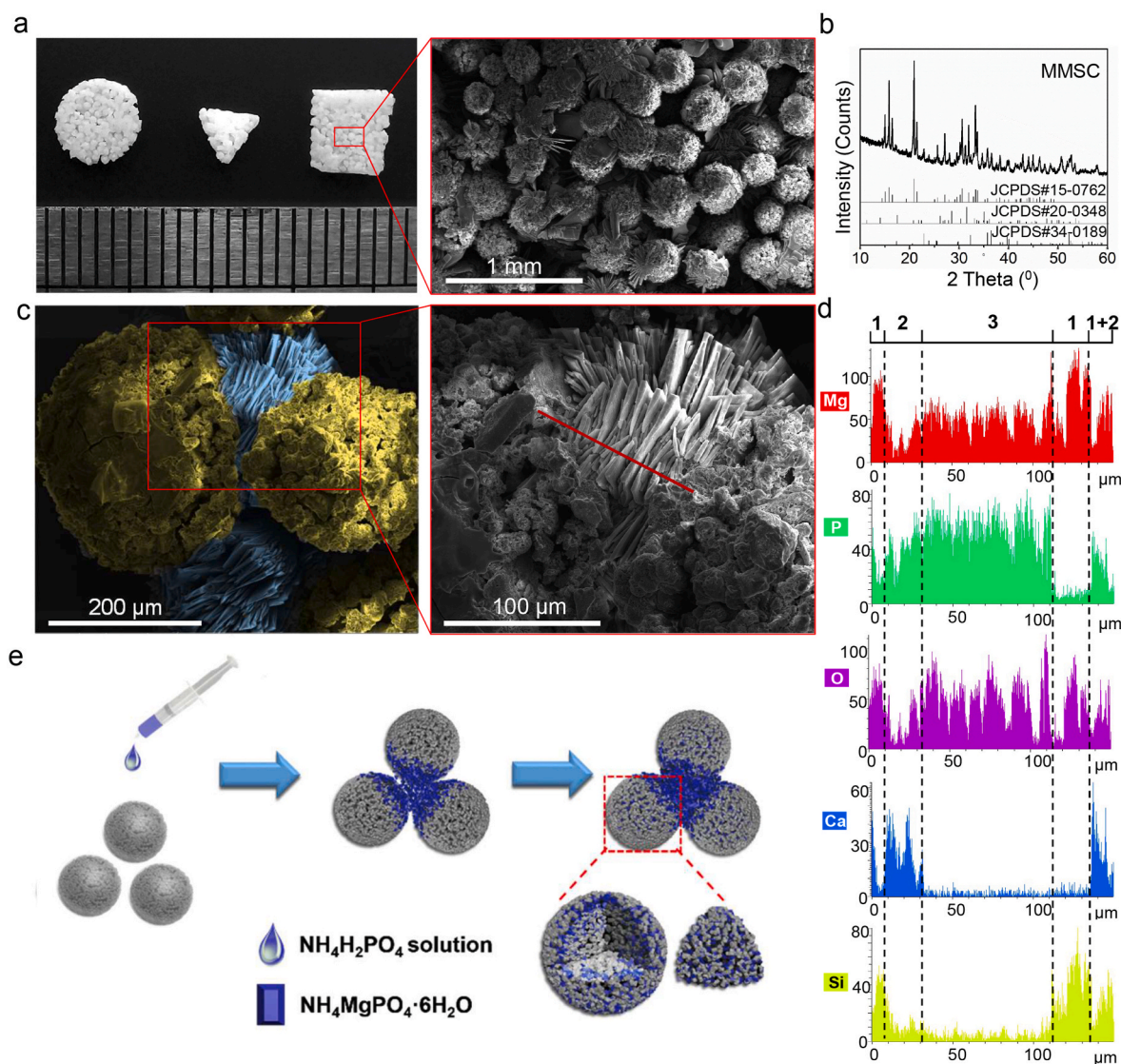


Fig. 3. Setting process of MMSC. (a) Digital photography and SEM images exhibited interconnected porous scaffolds with different 3D shapes cured by MMSC. (b) XRD results indicated that MgO within MMSs had reacted completely, and a new phase, $\text{NH}_4\text{MgPO}_4 \cdot 6\text{H}_2\text{O}$, formed after setting for 12 h compared with JCPDS#15–0762. (c) SEM image at a high magnification showed lamellar crystals formed between microspheres after setting for 20 min. (d) Element line scan results indicated that the phase composite of the lamellar crystals was $\text{NH}_4\text{MgPO}_4 \cdot 6\text{H}_2\text{O}$; 1, 2, and 3 pointed to the phases of MgO/Mg₂SiO₄, Ca₇Mg₂P₆O₂₄ and $\text{NH}_4\text{MgPO}_4 \cdot 6\text{H}_2\text{O}$, respectively. (e) Schematic diagram of the MMSC setting process.

which belonged to the curing product of MgO, whereas the phases Ca₇Mg₂P₆O₂₄ and Mg₂SiO₄ still existed in the cured MMSC scaffold (Fig. 3b). Since the curing reaction of commonly used bone cement, such as CPC and MPC, depends on the contact of powders with the setting liquid, we believed that the curing reaction of MMSs occurred gradually from the outside to the inside of the microsphere with the infiltration of the setting liquid. In this way, the phase transition and crystal growth preferentially occurred on the surface of the MMSs, leading to a concrectionary link at the contact interface of adjacent microspheres. In line with our assumption, we found lamellar crystals growing outwards parallel to the contact interface of the MMSs after setting for 20 min, which might be formed by the extrusion of the narrow space between the microspheres (Fig. 3c). Further, the X-ray EDS of such lamellar crystals demonstrated high Mg, P and O contents but almost no Ca and Si contents in this area (Fig. 3d). This result suggested that the lamellar crystals were $\text{NH}_4\text{MgPO}_4 \cdot 6\text{H}_2\text{O}$. We also found areas on the surface of MMSs adjacent to the lamellar crystals belonging to Ca₇Mg₂P₆O₂₄, Mg₂SiO₄ and unreacted MgO. The detailed elemental distribution is further shown in Fig. S5. Based on the above results, a schematic

diagram for the setting process that occurs preferentially at the contact interface of MMSs is proposed in Fig. 3e. Obviously, such a local preferential curing reaction mediated by microsphere provides great help for the formation of interconnected porous scaffolds.

3.2. MMSC was of desired physicochemical properties for clinical application

The physicochemical properties of an injectable bone cement need to meet certain requirements before it can be applied to the clinic. Injectability is a prerequisite for successful operation. According to the literature, spherical morphology may improve injectability [23] because of the lower plastic limit (PL) [24]. To verify whether the spherical morphology endowed MMSC paste with good rheological properties, the viscosity variation of cement slurry was determined (Fig. 4a). We noticed that the rheological property of the MPC could not be detected accurately because it cured too rapidly. In contrast, the rheological properties of MgO-based MMSC were not only detectable but also very stable. At the beginning of the test (shear rate from 100 s⁻¹ to 80 s⁻¹),

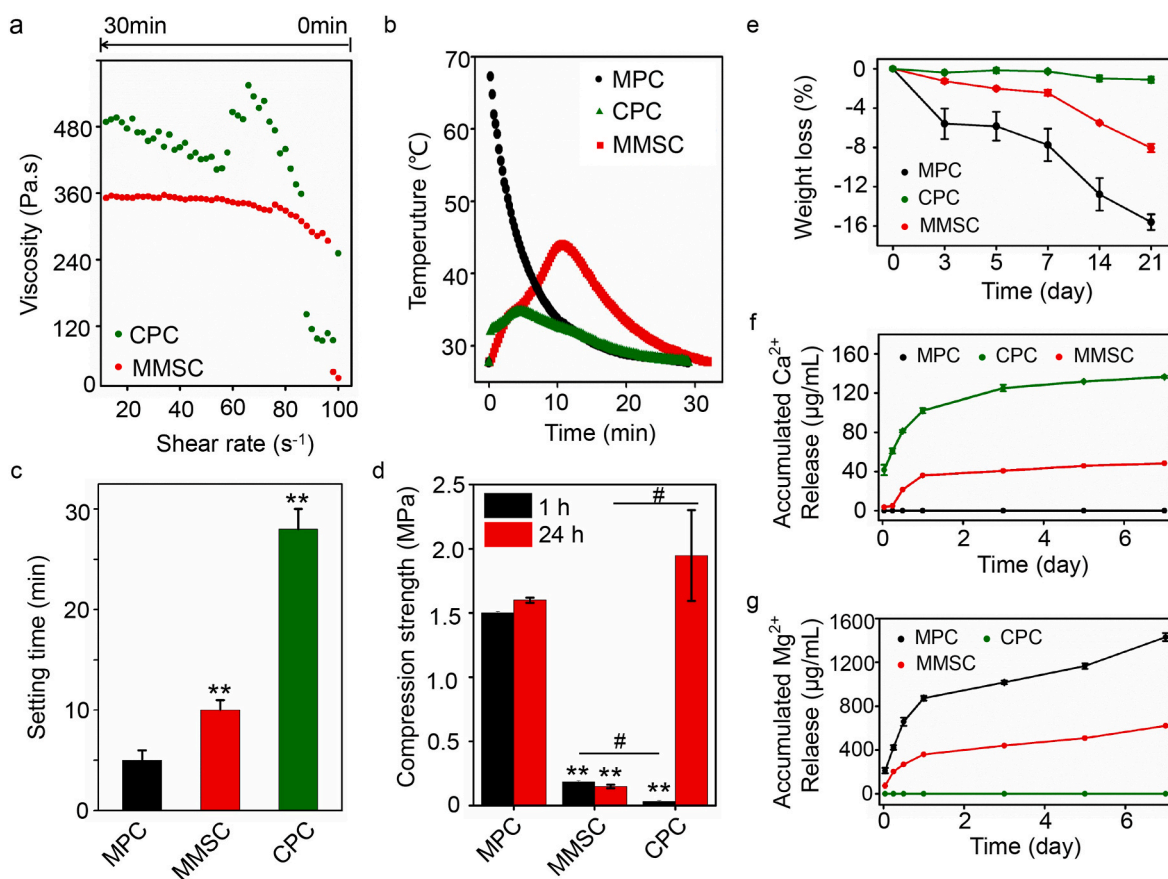


Fig. 4. Physicochemical properties of MMSC compared with those of the MPC and CPC. (a) The rheological curve showed that the MMSC pastes had a constant and low viscosity, which suggested good rheological properties and practicable injectability. (b) The heat release of MMSC was well-controlled in comparison with MPC suggesting that the microspheres effectively reduced the exothermic reaction (c) The setting time was approximately 10 min in the MMSC, which well-met the requirement of clinical application. (d) Mechanical strength results showed that the compressive strength of the MMSC was stable after setting for 1 h (mean \pm SD; $n = 3$; *significant difference compared with the MPC group, * $p < 0.05$, ** $p < 0.01$; # significant difference between groups, # $p < 0.05$). (e) MMSC had a moderate degradation rate with a weight loss of approximately 8 wt% after 21 days (mean \pm SD, $n = 5$). (f, g) Calcium and magnesium ions can be released from the MMSC simultaneously at a moderate rate (mean \pm SD, $n = 5$).

the viscosity of the MMSC paste immediately increased and was higher than that of the CPC paste. This could be attributed to the inherent rapid reaction rate of MgO within the MMSs. However, when the shear rate was lower than 80 s^{-1} , the viscosity of the MMSC paste remained almost constant and lower than that of the CPC paste, which severely varied with a decreasing shear rate [25]. The stability of the rheological property of the MMSC paste indicated that the small contact interface made a weak connection between the microspheres before curing was completed. Under the shearing force, the curing of the MMSC was likely to be a dynamic process of disconnection and linkage of the microspheres, leading to an excellent rheological property and injectability that is beneficial for clinical practice.

The curing reaction exotherm of bone cement directly affects its biocompatibility. We found that the CPC showed the lowest heat release, whereas the temperature of the MPC reached $70 \text{ }^\circ\text{C}$ instantly (Fig. 4b). Such severe heat release from the MPC is very likely to burn the peripheral tissue [26]. Although the main composition of MMSC was MgO, the heat release of MMSC was well controlled and much milder than that of MPC. The highest temperature of MMSC was approximately $45 \text{ }^\circ\text{C}$, and the time span above $40 \text{ }^\circ\text{C}$ was approximately 3 min, which was tolerable and can be regarded as a short, local high fever. In addition, at the initial stage of the curing reaction, both MPC and CPC powder showed instantaneous heat release, while the exotherm in MMSC increased consecutively. These results suggest that the spherical morphology of the MMSs reduced the reaction interface of MMSC, thereby moderating the heat release.

To our knowledge, injectable bone cement should be cured in situ, and the setting time is ideal within 8–15 min [27]. A setting time that is too short may impede the injection, while a setting time that is too long may prolong the operation and increase the suffering of patients. We found that the setting time of the MPC was approximately only 5 min (Fig. 4c), while it was excessively long for the CPC at approximately 30 min. The MMSC exhibited a setting time of approximately 10 min, which could satisfy the clinical demand. We further detected the compressive strength after setting for 1 h and 1 day (Fig. 4d). There was no obvious difference between the compressive strength of 1 h and 1 day setting in the MMSC and MPC, whereas a significant increase in compression strength was found in the CPC. These results demonstrate that MMSC have both an ideal setting time and stable mechanical properties after curing.

Ideal bioactive bone cement not only needs to fill the bone defect to provide the necessary mechanical support but also needs to provide sufficient space and bioactive ions to induce the ingrowth and regeneration of new bone tissue [28]. This requires appropriate biodegradation and ion release from the cured bone cement. The weight loss of the CPC, MPC and MMSC was detected by soaking the cured cement in DMEM solution for 3 weeks to determine the biodegradability (Fig. 4e). We found almost no weight loss in the CPC, while the weight loss of the MPC was up to approximately 16%. The MMSC had a moderate degradation rate, and only 8% weight loss was found after 3 weeks of incubation. The surface morphological changes and the phase transition of the cements before and after soaking in DMEM demonstrated that

degradation and remineralization occurred simultaneously (Fig. 3a, S6 and S7). However, by subcutaneous implantation (Fig. S8), we found that the *in vivo* degradation of the cements showed no obvious remineralization. Such differences may be due to the different environments *in vivo* and *in vitro*. We also found two unchanged phases of Mg_2SiO_4 and $Ca_7Mg_2P_6O_{24}$ in the MMSC, which might help slow biodegradation, thereby moderating the release of Mg^{2+} ions, providing a certain level of

Ca^{2+} ions and maintaining a porous structure in the MMSC compared with that in the MPC (Fig. 4f and g). Studies have shown that the rapid degradation of the MPC will lead to the alkalization of the surrounding environment, resulting in cell and tissue necrosis [29]. Moreover, high concentrations of Mg^{2+} ions may lead to severe inflammation and hinder tissue repair, whereas lower concentrations can induce immune responses that are conducive to tissue repair [11,14]. Here, by introducing

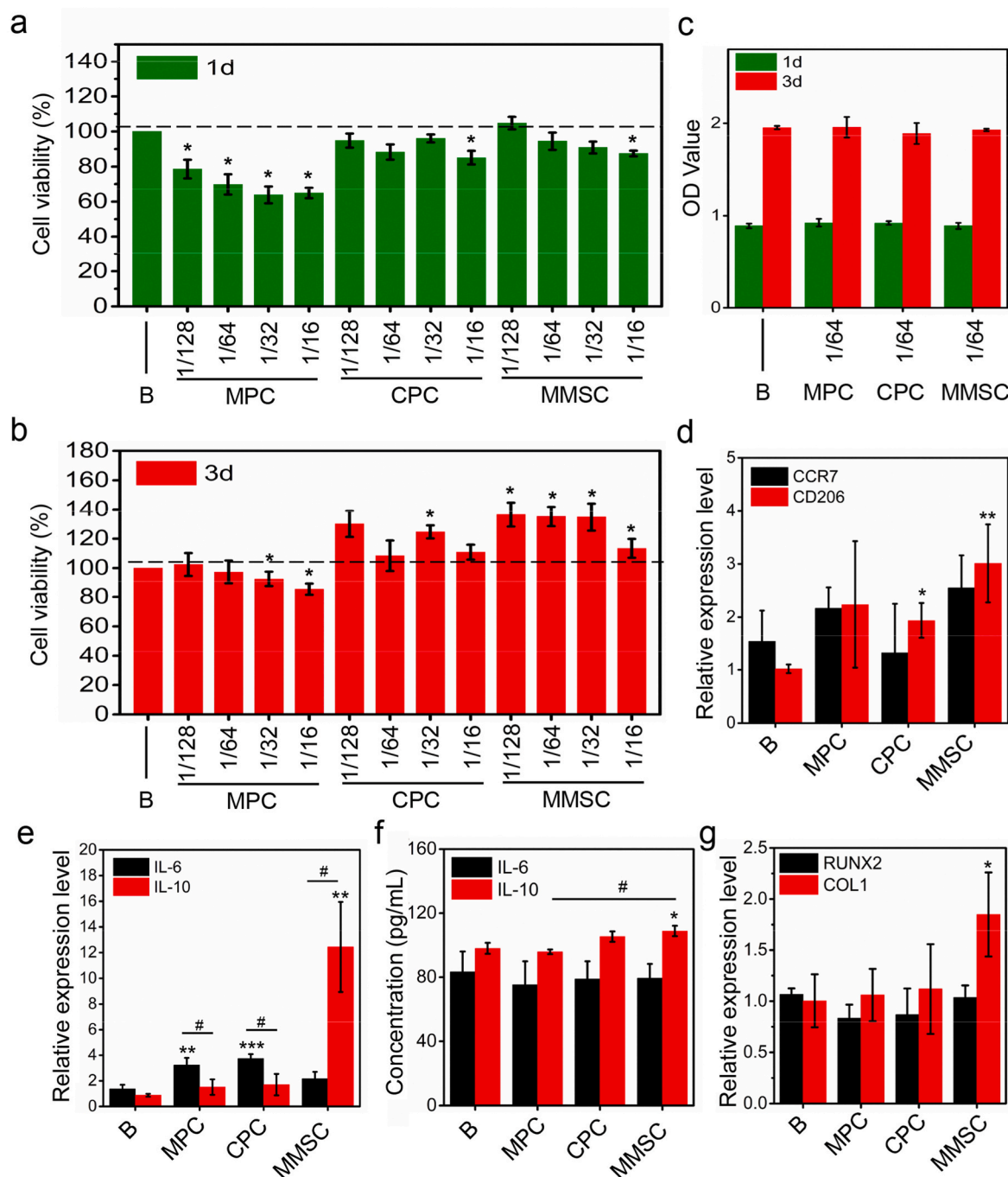


Fig. 5. *In vitro* cytocompatibility, immunoregulation and osteogenic induction. (a, b) CCK-8 assay showed all cement extracts with concentration ≤ 3.125 mg/mL were of no cytotoxicity to RAW264.7 cells. B: DMEM; 128, 64, 32, and 16 represent 1/128, 1/64, 1/32 and 1/16 of the original extract concentration (200 mg/mL), respectively. (c) Cement extracts with a concentration of 3.125 mg/mL had no cytotoxicity on rBMSCs. (d, e) RT-PCR results showed that the relative expression levels of CD206 and IL-10 significantly upregulated in RAW264.7 cells treated with MMSC extract at a concentration of 3.125 mg/mL, whereas the relative expression levels of IL-6 were significantly higher than IL-10 in the MPC and CPC groups. (f) ELISA tests revealed that the concentration of IL-10 in the MMSC group was significantly higher than that in the B and MPC group in the coculture system of RAW264.7 cells and rBMSCs. (g) RT-PCR results demonstrated that the relative expression level of COL1 in the MMSC group was upregulated and significantly higher than that in the B group in the coculture system (mean \pm SD; n = 3; *significant difference compared with the B group, *p < 0.05, **p < 0.01, ***p < 0.001; # significant difference between groups, #p < 0.05).

Mg₂SiO₄ and Ca₇Mg₂P₆O₂₄, the MMSC not only moderated the degradation of materials and controlled the release of Mg²⁺ ions but also provided additional Ca²⁺ ions, which simulated the nature of multiple elements in bone. Thus, the MMSC may have a great capability to promote the regeneration of new bone tissue.

3.3. MMSC extract triggered anti-inflammatory immunoregulation to promote osteogenesis *in vitro*

As a foreign body, implanted bone cement inevitably triggers an immune response that manipulates the subsequent biological behaviour of bone repair. A successful bone implant-induced *de novo* bone formation process consists of three consecutive phases [30]: the early phase of coagulation and acute inflammation, the bone formation phase of momentary chronic inflammation and osteogenesis, and the bone remodelling phase. However, a failure of bone implants usually represents a long period of chronic inflammation in the second phase, resulting in fibrous encapsulation of the materials. Many studies have shown that an in-time and effective switch from M1 to M2 macrophages plays an important role in the rapid and smooth transition from chronic inflammation to new bone formation [31,32]. Thus, bone cement has immunomodulatory properties, which lead to favourable M2 phenotype polarization may result in satisfactory osteogenesis. Herein, we examined whether MMSC could mediate the immune response in favour of bone repair by modulating the polarization of macrophages *in vitro*. The concentration of cement extracts used in the detection of the immune response of RAW 264.7 macrophages was determined to be 3.125 mg/mL according to the *priori* cytotoxicity study (Figs. 5a, 5b, S9). The cement extracts at such concentrations showed no obvious cytotoxicity in either RAW 267.4 macrophages or rbMSCs (Fig. 5c). We also found that compared with the control, the extracts of MMSC at a concentration of less than 12.5 mg/mL significantly enhanced the activity of RAW 264.7 macrophages after 3 days of cultivation. Further studies on the inflammatory genes demonstrated that MMSC extracts significantly increased the relative expression levels of CD206 and IL-10 without showing obvious effects on CCR7 and IL-6, whereas compared with the control, the CPC and MPC significantly promoted the level of IL-6 (Fig. 5d and e). Further flow cytometry experiments also showed that MMSC conditioned medium resulted in a shift toward the M2 phenotype with more RAW 264.7 macrophages expressed the surface marker CD206 (Fig. S10). Additionally, the expression level of IL-10 was dramatically higher than that of IL-6 in RAW 264.7 macrophages treated with extracts, while by contrast, the IL-10 level was substantially lower than that of IL-6 in both the CPC and MPC groups. To our knowledge, CCR7 and CD206 are representative surface markers of M1 and M2 macrophages, while IL-6 and IL-10 are proinflammatory and anti-inflammatory cytokines released from these two phenotypes of macrophages. Thus, our results clearly suggest a promotion of M2 phenotype polarization and anti-inflammatory cytokine expression by MMSC extract in RAW 264.7 macrophages. It was reported that the surface morphology of materials greatly affected the polarization of macrophages [33]. Therefore, we further investigated the influence of surface morphology of MMSC scaffold on macrophage polarization. The RT-PCR results showed that the surface morphology of MMSC scaffold exerted no significant effect on both the downregulation of IL-6 gene and the upregulation of IL-10 gene in comparison with MMSC extract (Fig. S11). This result indicated that it was the ions released from MMSC, typically Mg²⁺ ions, but not the morphology of MMSC that played the primary role in anti-inflammatory immunoregulation.

Given that the macrophage and bone cell interplay in the material-induced immune response and osteogenesis, indirect coculture of RAW 264.7 macrophages and rbMSCs was further conducted to concurrently investigate the influence of different bone cement extracts on both cells. Although the results showed no obvious difference in the IL-6 concentration among all four groups, compared with the control and MPC, the extract of the MMSC significantly increased the IL-10 concentration in

the coculture medium (Fig. 5f). Considering that recent study showed that IL-10 could promote the attachment, migration and osteogenic differentiation of mesenchymal stem cells [34], highly expressed IL-10 may promote the osteogenic differentiation of rMSCs. It has been reported that the difference in the concentration of Mg ions may alter the polarization of macrophages, leading to proinflammatory or anti-inflammatory effects [14]. Our results suggest that MMSC could provide and maintain a certain concentration of Mg ions in the coculture system, which was more conducive to the expression of anti-inflammatory cytokines than the MPC. Additionally, the expression of osteogenic genes, such as type I collagen, in the cocultured rbMSCs treated with MMSC extract was significantly increased compared with that in the control group (Fig. 5g). Considering that there was no osteogenic differentiation medium used in the coculture system, we speculated that the MMSC extract may promote the osteogenic differentiation of rbMSCs by regulating the expression of anti-inflammatory cytokines in macrophages.

3.4. MMSC exerted immunoregulation effect conducive to tissue repair and osteogenesis *in vivo*

Although the preceding *in vitro* experiments implied that MMSs could induce an M2-type favourable polarization of macrophages to reduce inflammation and to promote the osteogenic differentiation of rbMSCs, this effect was further validated in an ectopic bone formation model in rats. Macrophages differentiated from circulating monocytes usually arrive at the tissue injury site within 1–3 days, and their accumulation often peaks within 7 days; however, according to some studies, this process may be extended to 2–3 weeks [35]. Thus, by focusing on macrophages, we first evaluated the inflammatory response of the bone cements *in vivo* by subcutaneous implantation for 3, 7 and 14 days.

After 3 days of implantation, all three bone cements were surrounded by aggregated immune cells (Fig. 6 and Fig. S12). However, the porous structure of MMSC allows immune cells to penetrate the interstices of the microspheres instead of being blocked on the surface of the nonporous MPC and CPC. This was also confirmed by the SEM images of cross section of cements after 7 days of implantation (Fig. 6g–i). We also found obvious time-dependent biodegradation in the MMSC and MPC groups, while the CPC showed no evident biodegradation within two weeks, and the immune cells gathered on the surface of the CPC were gradually replaced by a layer of compact fibrous tissue during the 14 days of implantation (Fig. 6m–o). Since day 3, immune cell infiltration was observed at the material/cell interface of the MPC and MMSC. However, the biodegradation of the MPC was not rapid enough to allow complete cell penetration to the interior of the material within 14 days (Figure 6m). In addition, MPC degradation seemed to induce the accumulation of an increasing number of immune cells, resulting in aggravation of inflammation. In contrast, from day 7, the cells were found not only throughout the porous MMSC but also in the microspheres, and obvious vascular growth was also observed in the space between the microspheres (Figure 6o). Further immunohistochemical staining of α -smooth muscle actin (α SMA) (Fig. S13) showed mature blood vessels inside the MMSC indicating an initial tissue repair process. By the 14th day, most of the interconnected pores in the MMSC scaffold were filled with neo-tissues. More importantly, immune staining study (Fig. 7 and Fig. S14) demonstrated that although there were also a large number of macrophages located in the MMSC, the number of M2 type macrophages (CD163-positive staining) increased as time and were significantly higher than that of M1 type macrophages (CD86-positive staining) compared with the number of macrophages located in the MPC and CPC. In addition, the gene level of anti-inflammatory cytokine, IL-10, which can be secreted by M2 type macrophages [36,37], was significantly higher in the peripheral tissue of MMSC than that of MPC (Fig. S15). These results indicate that the MMSC could not only induce the ingrowth of cells, tissues and neovascularization through its porous scaffold structure and good biodegradability but also regulate the M2

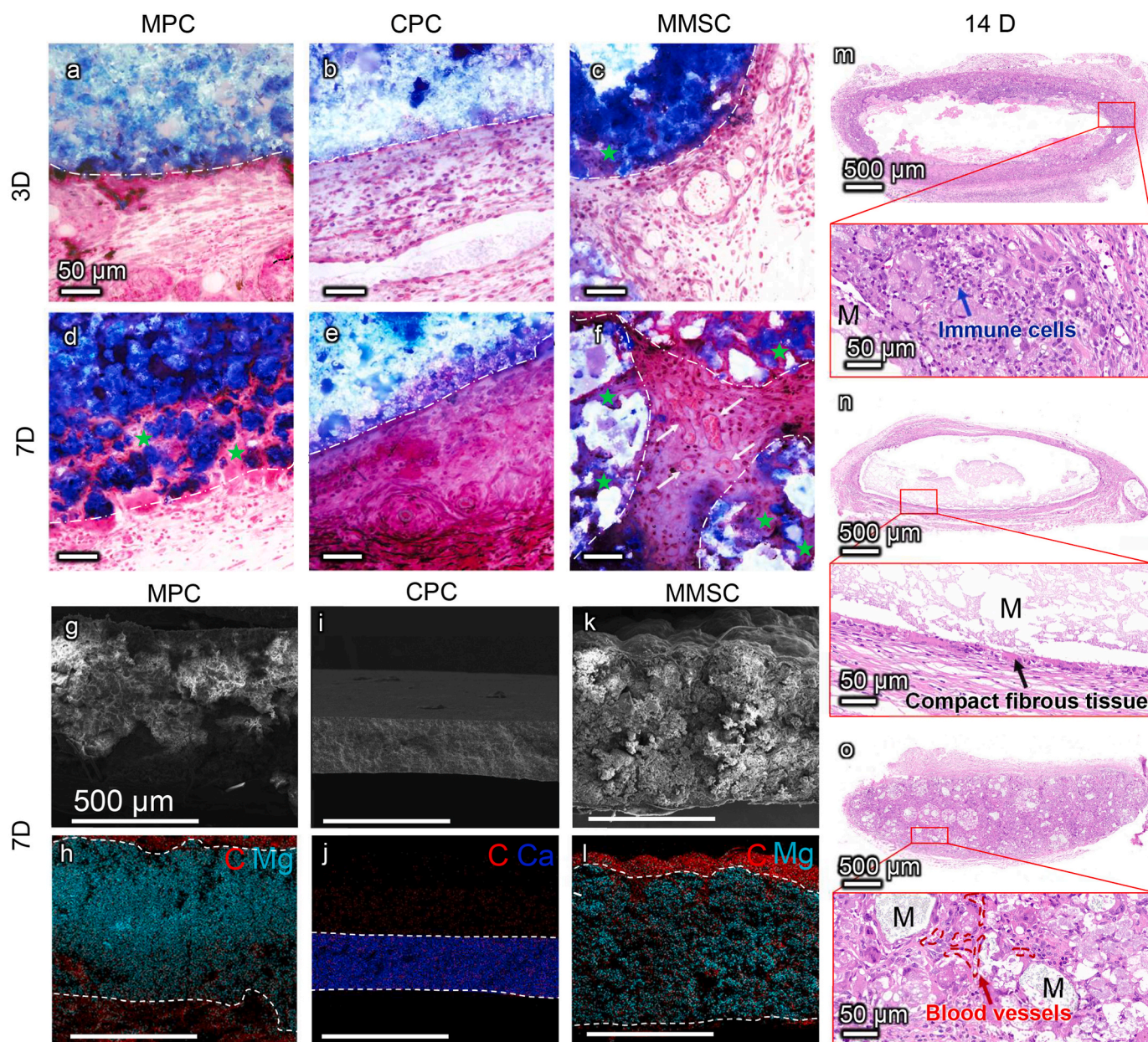


Fig. 6. Short-term immune response *in vivo*. Masson staining of MPC, CPC and MMSC subcutaneously implanted for 3 days (a, b, c) and 7 days (d, e, f). White dash lines portray the material boundaries. Green pentagrams indicate the cells infiltrated into the materials via the biodegradation of MPC and MMSC. White arrows point out the newly formed blood vessels in the gap of the MMSs. Scale bars are 50 μm. (g–l) SEM with elemental mapping images indicated the tissue ingrowth after 7 days of material implantation through the distribution of carbon elements (marked in red). White dotted lines describe the material boundaries. Scale bars are 500 μm. (m, n, o) HE staining of MPC, CPC and MMSC after 14 days of implantation. Aggregation of massive immune cells was observed surrounding the incompletely degraded MPC, while the CPC with no obvious degradation was encapsulated by compact fibrous tissues. By contrast, continuous ingrowth of cells and blood vessels took the space provided by the degradation of the microspheres in MMSC.

polarization of macrophages, which is conducive to tissue repair.

Given that the inflammatory response of the material was studied by subcutaneous implantation, for consistency, we applied a widely used rhBMP-2-mediated rat subcutaneous ectopic osteogenesis model [38] to investigate the inductivity of MMSC on bone regeneration. After 12 weeks of implantation, no obvious new bone formation was found in the MPC and CPC. Instead, dense fibrous tissue with a thickness of 50–100 μm was observed wrapping around the periphery of the material (Fig. 8 a–f). According to the above inflammatory response study, fibrous encapsulation of CPC should be formed within the first two weeks after implantation, whereas that of the MPC might be induced by long-lasting chronic inflammation. By contrast, most of the MMSC had been

degraded and replaced by new tissues and cells. Rather than fibrous tissues, we observed osteoblasts surrounding the microspheres (Fig. 8 g–k). Moreover, a large area of new bone was found not only between the space but also inside the microspheres. Because the cumulative release of BMP-2 from these three bone cements showed minor differences (Fig. S16), which indicated an almost identical growth factor-mediated osteogenic environment, we considered that the success of the MMSC in inducing ectopic osteogenesis could be mainly attributed to its porous structure, good biodegradability and immunomodulatory properties beneficial to bone tissue repair.

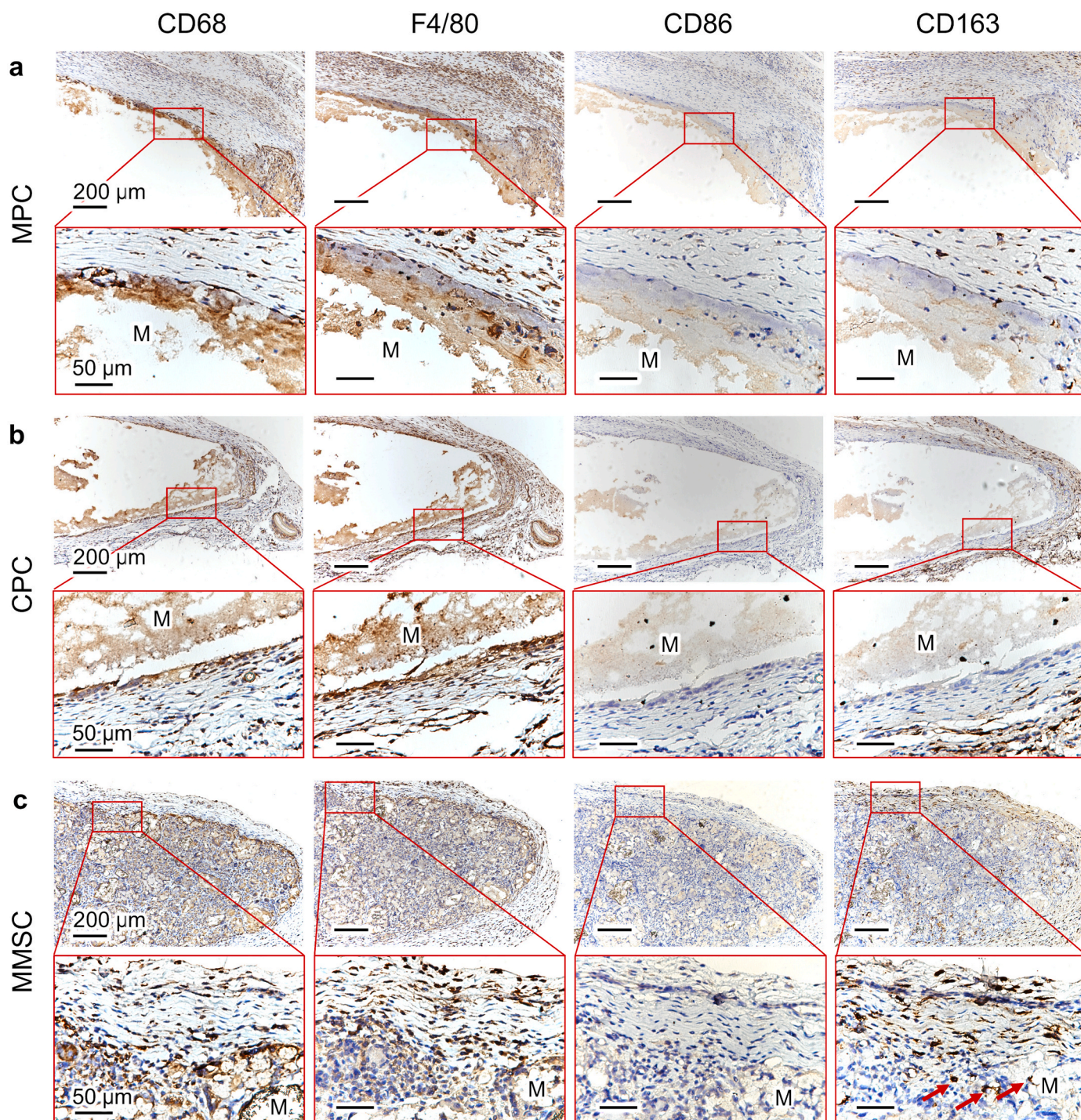


Fig. 7. Immunostaining of CD68, F4/80, CD86 and CD163 in the (a) MPC, (b) CPC and (c) MMSC after 14 days of material implantation. Red arrows pointed out the CD163-positive stained cells. CD68, F4/80, CD86 and CD163 are the cell markers of the immune cells, macrophages, M1 macrophages and M2 macrophages, respectively. The positive staining of these markers was found surrounding the MPC and CPC while inside the MMSC, demonstrating the porous structure of MMSC was beneficial to the inward migration of immune cells and macrophages. More importantly, CD163 was much more positive than CD86 in MMSC, which suggested a predominant M2 phenotype polarization of macrophages conducive to anti-inflammation and tissue repair induced by the MMSC.

4. Conclusion

In summary, we successfully fabricated the MMSs by a modified droplet freezing method. The bone cement prepared using MMSs was able to be cured to a porous scaffold *in situ*, and its physiochemical properties met the clinical requirements for injectable bone cement. *In vitro* study suggested that the controlled biodegradation and Mg ions release of MMSC promoted the osteogenic differentiation of rbMSCs by

regulating the expression of anti-inflammatory cytokines in macrophages. Further *in vivo* studies on inflammatory responses and ectopic bone formation demonstrated that the porous structure of MMSC facilitated the cell and tissue infiltration. Through biodegradation and release of magnesium ions, MMSC continuously provided space for more tissue ingrowth and exerted immunomodulation to induce anti-inflammatory M2 phenotype polarization of macrophages, angiogenesis and new bone formation. Therefore, with an interconnected 3D

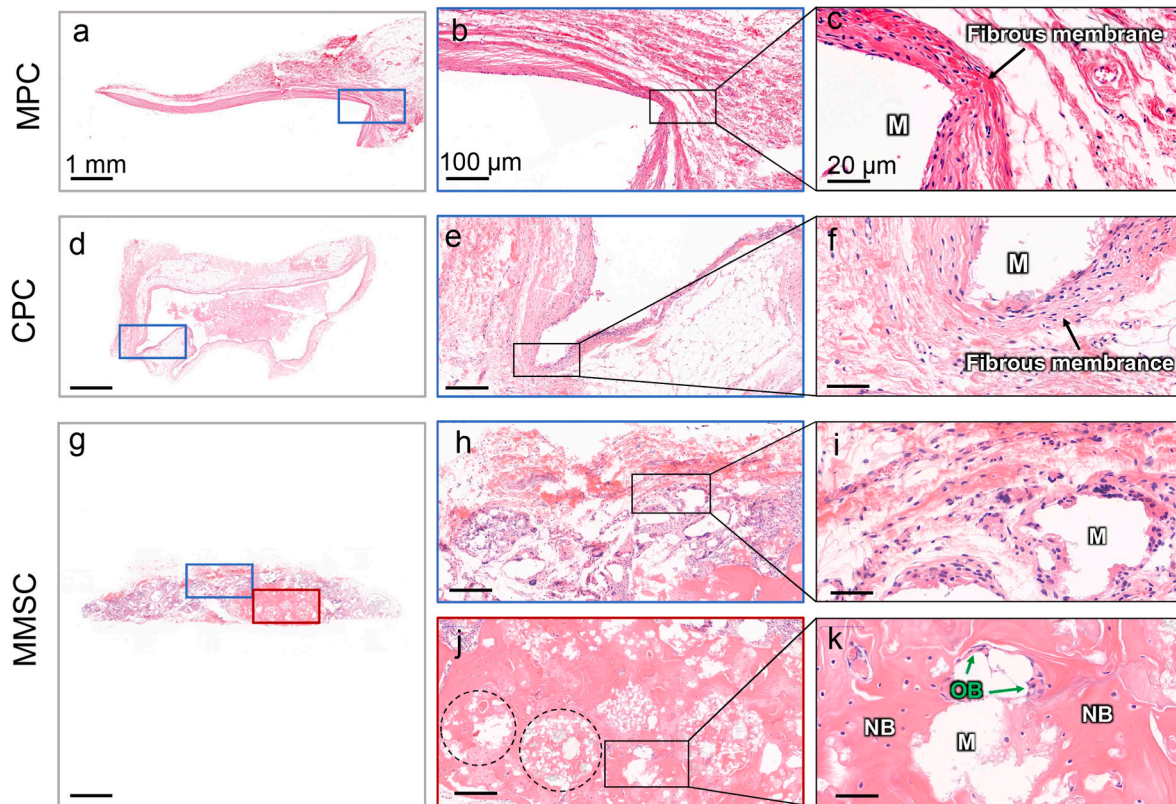


Fig. 8. Subcutaneous ectopic osteogenesis after 12 weeks of cements implantation. (a–f) No obvious new bone formation was found within the MPC and CPC, while they were encapsulated by dense fibrous membranes. (g–k) There was not only no obvious fibrous membrane encapsulating the MMSC, but also massive new bone formation was observed within the MMSC. Osteoblasts were also noticed at the boundaries of the incompletely degraded MMSCs. M: material; NB: new bone; OB: osteoblast; Dotted circle: microspheres with new bone.

porous structure, desired biodegradability, and anti-inflammatory immunomodulation, MMSCs bone cement has demonstrated excellent osteogenic capability, further envisioning its future application in bone tissue repair and regeneration.

CRedit authorship contribution statement

Shenglong Tan: contributed to the experimental planning, performed the experiments, Formal analysis, and . **Yifan Wang:** contributed to the experimental planning, performed the experiments, Formal analysis, and . **Yingying Du:** Supervision, contributed to the intellectual input, and . **Yin Xiao:** Supervision, contributed to the intellectual input, and . **Shengmin Zhang:** Supervision, founded the project, contributed to the experimental planning, intellectual input, Writing – review & editing.

Declaration of competing interest

None.

Acknowledgments

This work was supported by the National Key R & D Project (2018YFC1105701), National Natural Science Foundation of China (81801850, 81901897, 31870960) and China Postdoctoral Science Foundation Grant (2018M642851). We are also grateful to the Analytical and Testing Center of Huazhong University of Science and Technology for the assistance of analytical study of the project.

Appendix A. Supplementary data

Supplementary data to this article can be found online at <https://doi.org/10.1016/j.bioactmat.2021.03.006>.

References

- [1] N. Suhm, A. Gisepp, Injectable bone cement augmentation for the treatment of distal radius fractures: a review, *J. Orthop. Trauma* 22 (2008) S121–S125.
- [2] T.A. Russell, R.K. Leighton, Comparison of autogenous bone graft and endothermic calcium phosphate cement for defect augmentation in tibial plateau fractures, *J Bone Joint Surg-Am* 90A (2008) 2057–2061.
- [3] J.T. Zhang, W.Z. Liu, V. Schnitzler, F. Tancret, J.M. Bouler, Calcium phosphate cements for bone substitution: chemistry, handling and mechanical properties, *Acta Biomater.* 10 (2014) 1035–1049.
- [4] K.L. Low, S.H. Tan, S.H.S. Zein, J.A. Roether, V. Mourinho, A.R. Boccaccini, Calcium phosphate-based composites as injectable bone substitute materials, *J. Biomed. Mater. Res. B Appl. Biomater.* 94 (2010) 273–286.
- [5] Y. Li, J. Peng, L. Qin, T. Tang, M. Alini, B. Teng, et al., Osteogenic magnesium incorporated into PLGA/TCP porous scaffold by 3D printing for repairing challenging bone defect, *Biomaterials* 197 (2019) 207–219.
- [6] P. Lobenhoffer, T. Gerich, F. Witte, H. Tschernke, Use of an injectable calcium phosphate bone cement in the treatment of tibial plateau fractures: a prospective study of twenty-six cases with twenty-month mean follow-up, *J. Orthop. Trauma* 16 (2002) 143–149.
- [7] G. Mestres, M.P. Ginebra, Novel magnesium phosphate cements with high early strength and antibacterial properties, *Acta Biomater.* 7 (2011) 1853–1861.
- [8] M.E. Rodriguez-Ortiz, A. Canalejo, C. Herencia, J.M. Martinez-Moreno, A. Peralta-Ramirez, P. Perez-Martinez, et al., Magnesium modulates parathyroid hormone secretion and upregulates parathyroid receptor expression at moderately low calcium concentration, *Nephrol. Dial. Transplant.* 29 (2014) 282–289.
- [9] L. Galland, Magnesium and immune function: an overview, *Magnesium* 7 (1988) 290–299.
- [10] K. Brandao, F. Deason-Towne, A.L. Perraud, C. Schmitz, The role of Mg²⁺ in immune cells, *Immunol. Res.* 55 (2013) 261–269.
- [11] J. Shen, B. Chen, X. Zhai, W. Qiao, S. Wu, X. Liu, et al., Stepwise 3D-spatio-temporal magnesium cationic niche: nanocomposite scaffold mediated

- microenvironment for modulating intramembranous ossification, *Bioact Mater* 6 (2021) 503–519.
- [12] J.M. Anderson, A. Rodriguez, D.T. Chang, Foreign body reaction to biomaterials, *Semin. Immunol.* 20 (2008) 86–100.
- [13] Z. Chen, T. Klein, R.Z. Murray, R. Crawford, J. Chang, C. Wu, et al., Osteoimmunomodulation for the development of advanced bone biomaterials, *Mater. Today* 19 (2016) 304–321.
- [14] Z. Chen, X. Mao, L. Tan, T. Friis, C. Wu, R. Crawford, et al., Osteoimmunomodulatory properties of magnesium scaffolds coated with β -tricalcium phosphate, *Biomaterials* 35 (2014) 30.
- [15] C. Wu, Z. Chen, Q. Wu, D. Yi, T. Friis, X. Zheng, et al., Clinoenstatite coatings have high bonding strength, bioactive ion release, and osteoimmunomodulatory effects that enhance *in vivo* osseointegration, *Biomaterials* 71 (2015) 35–47.
- [16] F. Wu, J. Su, J. Wei, H. Guo, C. Liu, Injectable bioactive calcium-magnesium phosphate cement for bone regeneration, *Biomed. Mater.* 3 (2009) 4855–4863.
- [17] Y. Du, H. Liu, Q. Yang, S. Wang, J. Wang, J. Ma, et al., Selective laser sintering scaffold with hierarchical architecture and gradient composition for osteochondral repair in rabbits, *Biomaterials* 137 (2017) 37–48.
- [18] M.P. Ginebra, E. Fernández, M.G. Boltong, O. Bermúdez, J.A. Planell, F.C. M. Driessens, Compliance of an apatitic calcium phosphate cement with the short-term clinical requirements in bone surgery, orthopaedics and dentistry, *Clin. Mater.* 17 (1994) 99–104.
- [19] J. Zhang, X. Ma, D. Lin, H. Shi, Y. Yuan, W. Tang, et al., Magnesium modification of a calcium phosphate cement alters bone marrow stromal cell behavior via an integrin-mediated mechanism, *Biomaterials* 53 (2015) 251.
- [20] P. Xiong, Y. Dong, P. Lin, H. Wang, B. Liu, C. Guo, et al., Preparation of phosphate ceramic microspheres by the droplet freezing process, *J. Chin. Ceram. Soc.* 37 (2009) 436–440.
- [21] M. Sayer, A.D. Stratilatov, J. Reid, L. Calderin, M.J. Stott, X. Yin, et al., Structure and composition of silicon-stabilized tricalcium phosphate, *Biomaterials* 24 (2003) 369–382.
- [22] S. Langstaff, M. Sayer, T.J. Smith, S.M. Pugh, S.A.M. Hesp, W.T. Thompson, Resorbable bioceramics based on stabilized calcium phosphates. Part I: rational design, sample preparation and material characterization, *Biomaterials* 20 (1999) 1727–1741.
- [23] K. Ishikawa, Effects of spherical tetracalcium phosphate on injectability and basic properties of apatitic cement, *Key Eng. Mater.* 240–242 (2003) 369–372.
- [24] M. Bohner, G. Baroud, Injectability of calcium phosphate pastes, *Biomaterials* 26 (2005) 1553–1563.
- [25] C. Liu, H. Shao, F. Chen, H. Zheng, Rheological properties of concentrated aqueous injectable calcium phosphate cement slurry, *Biomaterials* 27 (2006) 5003–5013.
- [26] T. Udiljak, D. Ciglar, S. Skoric, Investigation into bone drilling and thermal bone necrosis, *Advances in Production Engineering & Management* 2 (2007) 103–112.
- [27] Y.J. No, S.I. Roohani-Esfahani, H. Zreiqat, Nanomaterials: the next step in injectable bone cements, *Nanomedicine* 9 (2014) 1745–1764.
- [28] J. Wei, J. Jia, F. Wu, S. Wei, H. Zhou, H. Zhang, et al., Hierarchically microporous/macroporous scaffold of magnesium–calcium phosphate for bone tissue regeneration, *Biomaterials* 31 (2010) 1260–1269.
- [29] B.S. Nagoba, N.M. Suryawanshi, B. Wadher, S. Selkar, Acidic environment and wound healing: a review, *Wounds A Compendium of Clinical Research & Practice* 27 (2015) 5–11.
- [30] F. Loi, L.A. Córdova, J. Pajarinen, T.H. Lin, Z. Yao, S.B. Goodman, Inflammation, fracture and bone repair, *Bone* 86 (2016) 119–130.
- [31] C. Schlundt, T.E. Khassawna, A. Serra, A. Dienelt, S. Wendler, H. Schell, et al., Macrophages in bone fracture healing: their essential role in endochondral ossification, *Bone* 106 (2018) 78–89.
- [32] I.M. Castaño, R.M. Raftery, G. Chen, B. Cavanagh, B. Quinn, G.P. Duffy, et al., Rapid bone repair with the recruitment of CD206+M2-like macrophages using non-viral scaffold-mediated miR-133a inhibition of host cells, *Acta Biomater.* 109 (2020) 267–279.
- [33] M.S. Joanna, F. Wei, J. Guo, J. Guillem-Marti, M.P. Ginebra, Y. Xiao, Effect of nano-structural properties of biomimetic hydroxyapatite on osteoimmunomodulation, *Biomaterials* 181 (2018) 318–332.
- [34] G. Vallés, F. Bensiamar, L. Maestro-Paramio, E. García-Rey, N. Vilaboa, L. Saldaña, et al., Influence of inflammatory conditions provided by macrophages on osteogenic ability of mesenchymal stem cells, *Stem Cell Res. Ther.* 11 (2020) 57.
- [35] M.L. Novak, E.M. Weinheimer-Haus, T.J. Koh, Macrophage activation and skeletal muscle healing following traumatic injury, *J. Pathol.* 232 (2014) 344–355.
- [36] T. Hanada, A. Yoshimura, Regulation of cytokine signaling and inflammation, *Cytokine Growth Factor Rev.* 13 (2002) 413–421.
- [37] Z. Chen, T. Klein, R.Z. Murray, R. Crawford, Y. Xiao, Osteoimmunomodulation for the development of advanced bone biomaterials, *Mater. Today* 4 (2015) 19.
- [38] J. Li, W. Zhi, T. Xu, S. Feng, K. Duan, J. Wang, Y. Mu, J. Weng, Ectopic osteogenesis and angiogenesis regulated by porous architecture of hydroxyapatite scaffolds with similar interconnecting structure *in vivo*, *Regen. Biomater.* 3 (2016) 285–297.